Chalcogenide Letters Vol. 15, No. 5, May 2018, p. 281 - 291

SYNTHESIS, STRUCTURAL AND OPTICAL CHARACTERIZATION OF CdS AND ZnS QUANTUM DOTS

A. GADALLA[a], M. S. ABD EL-SADEK[b], R. HAMOOD[*]
[a]*Physics Department, Faculty of Science,* 71516 *Assiut University, Egypt*
[b]*Nanomaterials Lab., Physics Department, Faculty of Science, South Valley University, Qena-83523, Egypt*

In the present work, we have employed an organometallic method for preparing CdS and ZnS nanoparticles (NPs). In the synthesis of CdS and ZnS, Cadmium Oxide, Zinc Oxide and Sulfur are used as precursors. X-Ray diffraction (XRD) pattern confirms that the sample is crystalline structure with a hexagonal wurtzite phase. X-ray peak broadening analysis was used to estimate the crystallite sizes and lattice strain using the Williamson-Hall (W-H) analysis. The crystallinity of the samples, lattice fringes and the formation of agglomerated nanoparticles clearly showed using the high resolution TEM technique. The elemental composition of CdS and ZnS are determined by energy dispersive X-ray spectroscopy (EDS). Fourier Transform Infra-Red spectra (FTIR) are measured for identification of chemical bonds in the nanomaterial, while Raman spectroscopy was performed to study the confinement of the optical phonon modes in the QDs. The diameters of particles are calculated using yu equation. These diameters are found to lie in the range of 2.62 - 2.73 nm for CdS and of 2.88 - 4.09 nm for ZnS NPs. Absorption peaks are red-shifted gradually as the particle size increased with an increment equals 5 nm for CdS and 19 nm for ZnS. Zinc sulfide NPs resulted better enhancement of the photoluminescence than that of Cadmium Sulfide NPs.

(Received February 27, 2018; Accepted May 18, 2018)

Keywords: CdS; ZnS; Quantum dots; XRD; HRTEM; Optical properties.

1. Introduction

Due to their electronic and fascinating optical properties, semiconductor quantum dots based on luminescence properties of II-VI group's elements have gained considerable attention to research community [1-5]. Because of their fundamental role in basic research and technological applications, synthesis and characterization of discrete nanostructures is of significant importance [6]. Regarding their applications, it is a generally recognized that their large surface to volume ratio enhance surface effects which result in novel phenomena. Accordingly, nanobuilding materials such as ZnO nanowires, GaN nanowires, ZnS nanoparticles, CdS nanoparticles and Carbon nanotubes are intensively investigated [5, 6]. At the nanoparticles sizes of semiconductors, some of the physical properties noticeably differ from those of the corresponding bulk materials, for instance, the energy gap increases and the optical spectrum is shifted toward the short-wavelength region [7].

Cadmium sulfide (CdS) nanoparticles possess various applications in display devices, solar cells and as photocatalyst [8, 9]. Recent research on nanoparticles have shown that they could stand as potential candidates for electronic and optoelectronic applications. It is worth mentioning too, that synthesis, characterization and studies of optical properties of cadmium sulfide have been researched, analyzed and described by several research groups [10-13]. CdS is a wide band gap semiconducting material with band gap of 2.49 eV and it's widely used because of its size dependent photophysical and non-linear optical properties. [14-16].

[*]Corresponding author: rananom77@yahoo.com

Zinc sulfide (ZnS) is an important II-VI group semiconductor material with a direct band gap of 3.86 eV and is widely used as phosphor in photoluminescence (PL), electroluminescence (EL) and optical sensor because of its chemical stability compared to those other chalcogenides such as ZnSe [1]. It, futher, exhibits wide optical transparency from the visible light (0.4 μm) to the deep infrared region (12 μm) which makes ZnS as one of the most promising materials among II-VI groups.

The synthesis of CdS and ZnS nanoparticles have been synthesized by many various methods, some of which are the direct reaction of metals with sulfur powder under high temperature; the thermal decomposition of molecular precursors containing M-S bonds [17]; the use of poisonous H_2S as S^{2-} source at higher temperature [18] and finally the chemical co-precipitation method [19].

In this work, CdS and ZnS nanoparticles have been synthesized by organometallic method [20] using CdO and ZnO as precursors and TOPO (Trioctylphosphine oxide) as capping agent to control the particle sizes. The main attention is paid to the synthesis CdS and ZnS NPs in order to distinguish between the differential characterization of CdS (low energy band) & ZnS (high energy band) [21]. The crystallinity and morphology have been studied by using X-ray powder diffraction (XRD) and high resolution transmission electron microscope (HRTEM). The vibrational structure has been approved by using FTIR and Raman spectroscopy. The absorption spectra and the photoluminescence (PL) emission properties of CdS and ZnS samples are recorded.

2. Experimental

2.1. Synthesis of CdS and ZnS Nanocrystals by Organometallic Method

Pure Sulfur powder as a Sulfur source, and all the chemicals that will be mentioned later are of analytical grade and used without further purification. The experimental setup that has been used in the preparation of CdS and ZnS nanoparticles consisted of a glass round bottom flask on heating mantle maintained at 170 °C. CdO and ZnO were used as starting materials to synthesis CdS and ZnS NPs by various sizes. The weight amounts of 0.3 g CdO or ZnO have been solved in (3 ml) Oleic acid, then heated up to 170 °C with continuous stirring. A mixture of (2 g) TOPO and (2 g) HDA (Hexadecylamine) has been added and then the temperature has been increased up to 220 °C. When the solution became transparent, the temperature was decreased to 190 °C. Trioctylphosphine sulfur (TOP-S) solution was injected. Four samples of CdS were withdrawn at different time intervals (5, 15, 20 & 30 min) and labeled from (a to d). At the same intervals, four samples of ZnS labeled from (1 to 4) were withdrawn. Drawn samples were cooled and diluted by the addition of toluene. The samples b of CdS and 2 of ZnS were centrifuged at (4000 rpm, 15 min) and the obtained precipitates were washed three times by acetone and methanol. The obtained powders are characterized by XRD to confirm the crystalline phase and size.

3. Results and Discussion

3.1 Structural and Morphology

The typical XRD pattern of the prepared samples of CdS and ZnS nanoparticles is shown in Fig. 1.

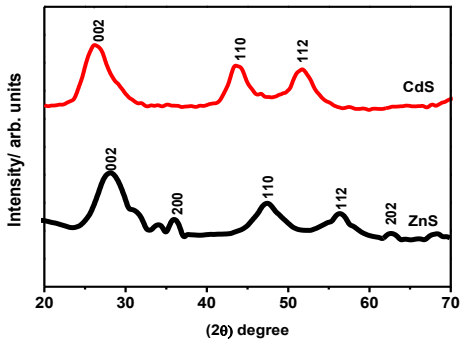

Fig. 1. X-ray powder pattern diffraction collected on two different samples: CdS (sample b) and ZnS (sample 2) nanoparticles

XRD were determined by using wide-angle X-ray scattering; Philips PW 1710 monochromatic Cu-K_α radiation with (λ = 1.54056 Å). The diffraction peaks were indexed to hexagonal phased of CdS and ZnS QD's with major (hkl) peaks at (002), (110) and (112) respectively, and the lattice constants were found to be a = 4.15, c = 6.78 for CdS while a = 3.83, c = 6.38 for ZnS as represented in JCPDS cards nos. (04-017-1120) (04-017-6151) respectively. There are broad peaks indicating the nanocrystalline behavior of the particles. The grain size has been estimated from the broadening of the most intense peak (002) using Debye-Scherrer formula [22]:

$$L = K\lambda/\beta_D cos\theta \tag{1}$$

In which L is the coherence length, β_{hkl} is the full width at half maxima (FWHM) of the diffraction peak (in radiant), λ is the X-ray wavelength, θ is the angle obtained from 2θ value corresponding to maximum intensity peak pattern and K is the geometric factor (0.9). In case of a small crystallites; L = 3/4 D, where D is diameter of nanoparticles. The grain size for CdS nanocrystals has been obtained 3.34 nm while its value for ZnS was 2.95 nm. The measured lattice constants, d-spacing and particles size were reported in Table 1.

The strain and grain sizes of both samples CdS and ZnS were calculated by Williamson-Hall (W-H) method. In general, the local distortion of the lattice has generated strain in the lattice. Its contribution to peak broadening is well known as strain broadening. By considering the strain to be uniform deformation model (UDM) in all crystallographic directions, the strain broadening can be written as [23, 24]:

$$\varepsilon = \frac{\beta_{strain}}{4\ tan\theta} \tag{2}$$

The significant property of Equation (2) is the dependency on the diffraction angle θ. The Williamson-Hall method does not follow a $1/cos\theta$ dependency as in the scherrer equation, it instead varies with $tan\theta$. When both microstrain and microstructural causes-small crystallite size - occur together, a separation of reflection broadening has been allowed. The distinct θ dependencies of both effects laid the basis for the separation of size and strain broadening in the analysis of Williamson and Hall results in the following equations [23, 25]:

$$\beta_{hkl} = \beta_D + \beta_{strain} \tag{3}$$

By substituting the values for β_D and β_{strain} in Eq. (3)

$$\beta_{hkl} = \left(\frac{k\lambda}{Dcos\theta}\right) + 4\varepsilon\, tan\theta \quad (4)$$

By rearranging Eq. (4) we get:

$$\beta_{hkl}\, cos\theta = \left(\frac{k\lambda}{D}\right) + 4\varepsilon\, sin\theta \quad (5)$$

The term 4 sin Θ is plotted along the x-axis and $\beta_{hkl}\ cos\theta$ along the y-axis for the synthesized CdS and ZnS NPs as it is shown in Fig. 2a, b. From the linear fit of the data, the strain was calculated from the slope of the graph and the particle size D has been estimated by the Y-intercept [23, 25]. The calculated average crystallite sizes estimated from Scherrer method and UDM model with strain are listed in Table 1.

Table 1. The X-ray analysis of CdS and ZnS nanoparticles by Scherrer and Williamson-Hall

Sample	2θ °of the intense peak	FWHM (degree)	(hkl)	d-spacing (Å) Std.	d-spacing (Å) Obs.	Cell Const. a (Å)	Cell Const. c (Å)	Scherrer equ.	Williamson-Hall method	
								D (nm)	D (nm)	$\varepsilon \times 10^{-2}$ (no unit)
CdS	26.2	3.58	(002)	3.32	3.37	4.15	6.78	3.34	2.02	1.78
ZnS	28.24	4.23	(002)	3.15	3.16	3.83	6.38	2.95	3.73	1.27

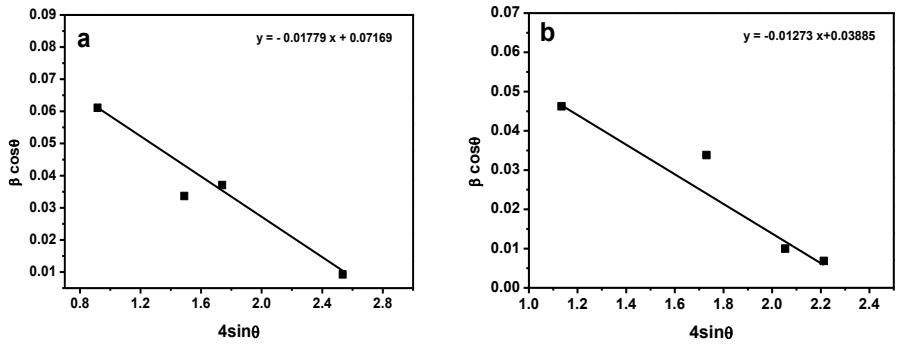

Fig. 2. The W-H analysis of (a) CdS, (b) ZnS

The purity of the samples and the precise composition were determined by an EDS study. Fig. 3 indicates the energy dispersive spectrum (EDS) of the CdS and ZnS nanoparticles which have been investigated by EDS (JEOL JSX 3222 element analyzer). It shows the unambiguous evidence for the presence of Cd/ S and Zn/S components. From the EDS spectrum, it has been realized that atomic weight ratios of Cd and S in the CdS NPs were around 58.93 % and 41.07 %, respectively, Fig. 3a.The atomic weight ratios of Zn and S in the ZnS NPs were around 72.79 % and 27.21 %, respectively, Fig. 3b. No impurities were appeared in the structure.

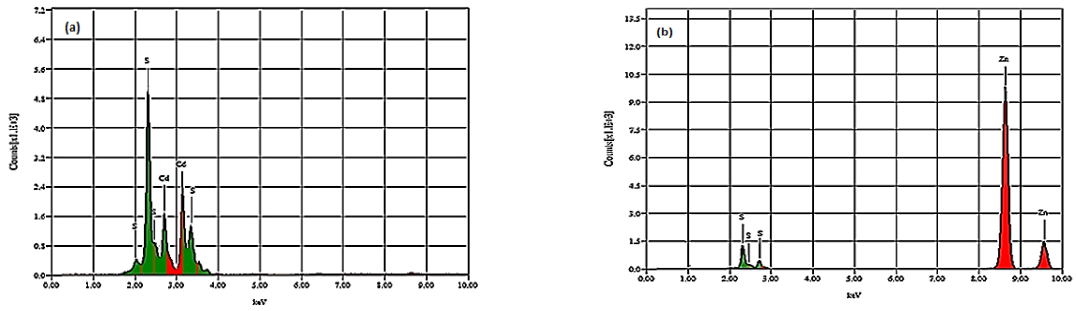

Fig. 3. EDS spectrum of (a) CdS and (b) ZnS NPs

Fig. 4 shows the high resolution transmission electron microscopy (HRTEM) images for CdS and ZnS NPs with their particles size distribution determined by using (JEM-2100 of 200KV). The TEM micrographs Fig. 4a show that the CdS nanoparticles were nearly spherical with some agglomeration. The average particle size is about 3.5 nm with a standard deviation of about 0.5 nm. The obtained value of the d-spacing calculated for CdS is equal to 0.20 nm assigned to (110) plane of hexagonal structure. Fig.4b shows homogenous distribution of ZnS NPs with no agglomeration. The lattice planes distance is identical to hexagonal ZnS, its calculated value equals to 0.24 nm assigned to (102) plane, and its average size from the histogram is equal to 3.75±0.3 nm.

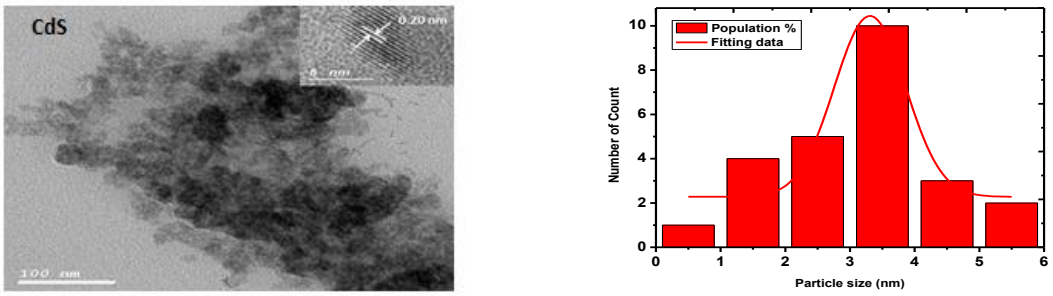

a)

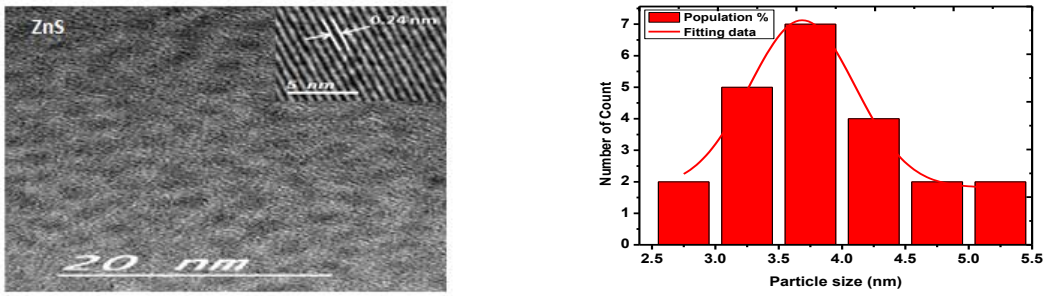

b)

Fig. 4. HRTEM images and size histogram for synthesis (a) CdS and (b) ZnS nanoparticles

By comparing the TEM micrograph of CdS and ZnS NPs; it is observed that the CdS NPs size is smaller than that of ZnS NPs. This is due to the higher surface to volume ratio of CdS than ZnS that tend to agglomerate to minimize its surface energy. Uncontrolled agglomeration of CdS nanoparticles may occur due to attractive Vander Waals forces between particles.

FTIR is an analytical technique used to identify information about the chemical bonding in a material. It is used to obtain the elemental constituents of a material [26]. Fig. 5a, b shows the

FTIR spectrum of TOPO capped CdS and ZnS nanoparticles at room temperature which was recorded by using (FT/IR spectrometer -4100 LE) in the range of 4000-500 cm^{-1}. Samples can be prepared by several ways for an IR measurement. For powders, a small amount of the sample is added to potassium bromide (KBr), after which this mixture is ground into a fine powder and subsequently compressed into a small, thin, quasi-transparent disc. The observed vibration peaks at (2929 & 2849 cm^{-1}) and at (2919 & 2847 cm^{-1}) are attributed to C-H stretching bands that confirm the capping of alkyl group over CdS and ZnS NPs, respectively. The peaks at 2354 cm^{-1} for CdS and 2499 cm^{-1} for ZnS are due to C-N vibrations. The peaks are observed at 1568 cm^{-1} for CdS and at 1557 cm^{-1} for ZnS NPs which are corresponding to C-O stretching [27]. Peaks appeared at 1493 cm^{-1} for CdS and at 1466 cm^{-1} for ZnS are attributed to COOH stretching. The peaks at 1062 cm^{-1} for CdS and 1047 cm^{-1} for ZnS are due to the presence of resonance interaction between vibrational modes of sulfide ions in the crystal. The peaks appearing at 723 cm^{-1} for CdS and at 731 cm^{-1} for ZnS are possibly due to Cd-S and Zn-S stretching vibrations.

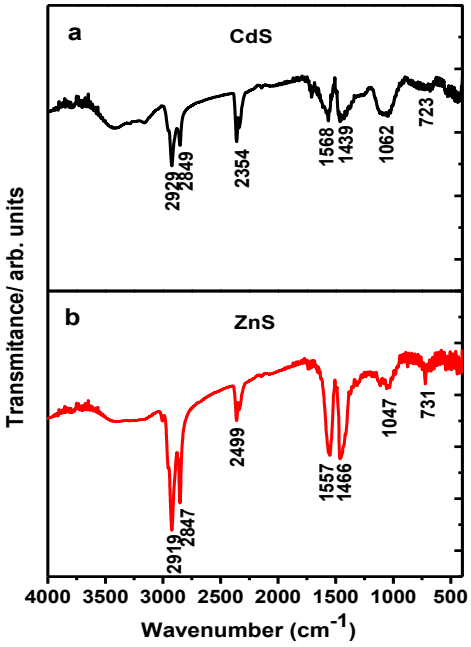

Fig. 5. FTIR spectra of the prepared a) CdS and b) ZnS NPs

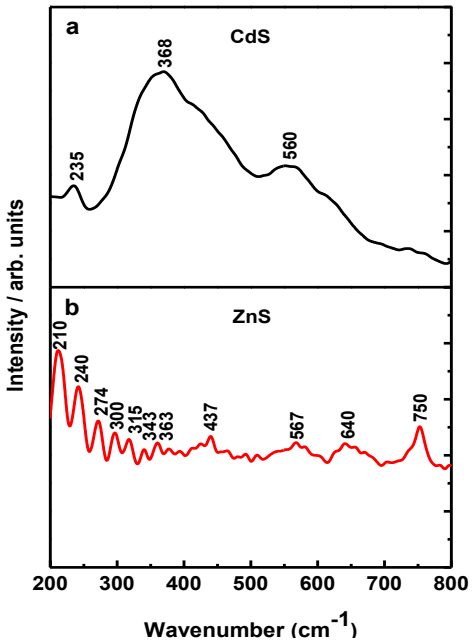

Fig. 6. Raman spectra of the prepared a) CdS and b) ZnS NPs

Fig. 6 shows the Raman spectra of CdS and ZnS nanoparticles at room temperature. In Fig. 6a, one peak is located at 235 cm^{-1} which corresponds to transverse optical (TO) phonon mode and two peaks are located at 368 & 560 cm^{-1} which correspond to fundamental bands related to stretching vibrations of longitudinal optical (LO) phonon modes of CdS 1LO and 2LO, respectively [22].

Fig. 6b shows a peak that at 210 cm^{-1} is due to the second order of longitudinal acoustic (2LA) phonon mode. The band at 240 cm^{-1} can be attributed to the combination of two phonons at w (2(0) at w). The peak observed at 274 cm^{-1} represents transverse optical (TO) phonon mode. The two other bands occur at 300 and 315 cm^{-1} are assigned to the same surface optical (SO) mode. The weak peak at 343 cm^{-1} is indicated to longitudinal optical mode (LO). The combination bands at 363, 437 and 567 cm^{-1} can be assigned to TO+LA, LO+TA and 2TO-TA, respectively. The peaks at 640 and 750 cm^{-1} correspond to 2TO and 2LO modes, respectively. Raman spectra were

recorded using Brucker Senerra Raman microscope (Bruker Optics Inc., Germany) with 785 nm excitation.

3.2. Optical Properties

The effects of concentration and time on the optical properties of the synthesized samples were evaluated by using a Perkin Elmer lambda 750 UV-Vis spectrophotometer in the wavelength range 300-700 nm. The optical absorbance versus wavelength traces for prepared CdS and ZnS nanoparticles samples are shown in Fig. 7.

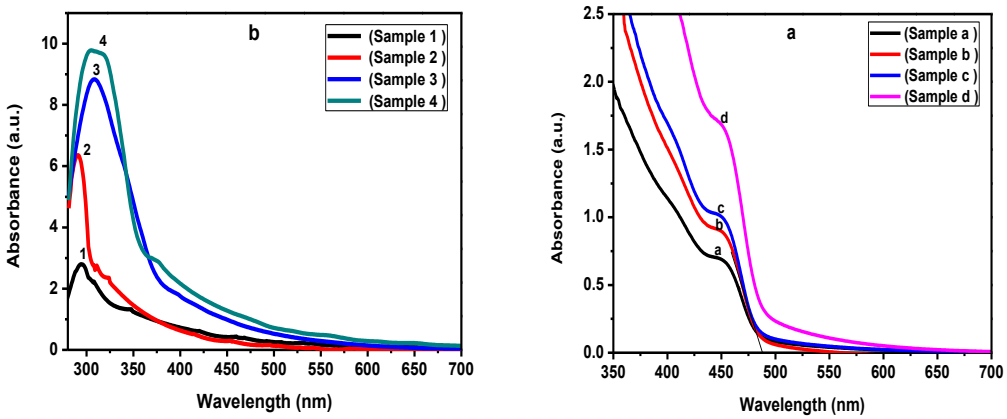

Fig. 7. Absorption spectra of different samples of (a) CdS and (b) ZnS nanoparticles

In Fig. 7a, the average particle size of CdS QDs was estimate by using the following Yu's et al. equation [28]

$$D = (-6.6521 \times 10^{-8})\lambda^3 + (1.9557 \times 10^{-4})\lambda^2 - (9.2352 \times 10^{-2})\lambda + 13.29 \quad (6)$$

In which D (nm) is the size of a given nanocrystal sample and λ (nm) is the wavelength of the first excitonic absorption peak of the corresponding sample [23]. The calculated diameters of CdS were found to be (2.62-2.73 nm) at the growth time ranging from (5-30 min). In this case, CdS is red shifted from 449-454 nm by an increment equals 5 nm. The average particle size of ZnS NPs was estimated from the following equation [29]:

$$r(nm) = -0.2963 + \sqrt{-40.1970 + \frac{13620}{\lambda_p}} \div \left(-7.34 + \frac{2481.6}{\lambda_p}\right) \quad (7)$$

In which r is the particle size and (λ_p) is peak absorbance wavelength. The calculated diameters of ZnS were found to be (2.88 – 4.09 nm) at the growth time was ranging from (5-30 min). It is observed that, the ZnS is a red shifted from 293-312 nm by difference equals 19 nm, Fig. 7b. Corresponding absorption edges due to the transition between the electronic state and the particle sizes for CdS and ZnS are reported in Table 2.

Table 2.1. Spectroscopy parameters of a) CdS and b) ZnS Nanoparticles

a) CdS						
Samp. No.	Reaction time (min)	$\lambda_{Abs.}$ (nm)	$\lambda_{Emi.}$ (nm)	Particle size (nm) Yu Eq.	X-ray size (nm)	HRTEM size nm
a	5	449	456	2.62	-	-
b	15	451	460	2.66	3.34	3.5
c	20	453	464	2.70	-	-
d	30	454	470	2.73	-	-

b) ZnS						
Samp. No.	Reaction time (min)	$\lambda_{Abs.}$ (nm)	$\lambda_{Emi.}$ (nm)	Particle size (nm) Yu Eq.	X-ray size (nm)	HRTEM size (nm)
1	5	293	454	2.88	-	-
2	15	294	-	2.93	2.95	3.75
3	20	310	463	3.91	-	-
4	30	312	466	4.09	-	-

The absorption which corresponds to electron excitation from the valence band to conduction band can be used to determine the nature and values of the optical band gap. The relation between the absorption coefficient (α) and the incident photon energy ($h\nu$) can be written as [30, 31]

$$(\alpha h\nu) = K(h\nu - E_g)^n \tag{8}$$

Where K, h, and E_g are a constant, the Planck's constant and the band gap respectively. For n=1/2, E_g in Eq. 8 is the direct allowed band gap [22]. To measure the energy band gap of CdS and ZnS NPs from the absorbance spectrum a graph $(\alpha h\nu)^2$ versus $h\nu$ is plotted in Fig. 8. The extrapolate of the straight line to $(\alpha h\nu)^2 = 0$ axis represents the E_g values of CdS and ZnS which were found to be 2.73 eV and 3.97 eV, respectively. The E_g of CdS NPs is blue shifted from its bulk value (E_g = 2.45 eV) with increment equals 0.24 eV [22]. As well as the E_g of ZnS NPs is blue shifted from its bulk value (E_g = 3.65 eV) with increment equals 0.32 eV [32], Table 3. That difference in band gap of the nanoparticles is due to the change in the ground state (bulk) to size dependence.

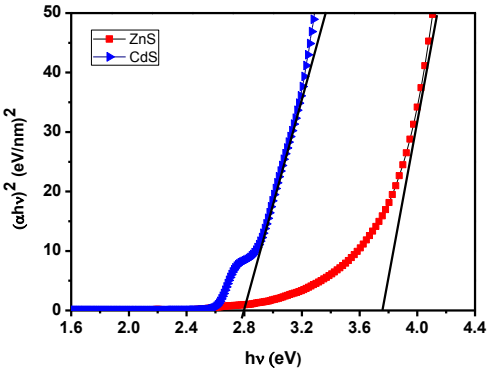

Fig. 8. Variation of $(\alpha h\nu)^2$ with $h\nu$ for CdS and ZnS NPs as a function of wavelength at n value of 1/2

Table 3. Band gap increment in CdS and ZnS quantum dots due to quantum confinement

Sample	Absorption edge (nm)	Band gap E_g (eV)	Increment in band gap (eV)
CdS Bulk	498	2.49	-
CdS Nano	454	2.73	0.24
ZnS Bulk	340	3.65	-
ZnS Nano	312	3.97	0.32

The room-temperature photo-luminescent (PL) spectra of the prepared CdS and ZnS Quantum Dots (QDs) measured by using JASCO-FP-6300 fluorescence spectrometer were shown in Fig. 9. Excellent capping of (TOPO) is effectively passivated CdS and ZnS samples. In the present investigation, fluorescence spectra were performed with an excitation wavelength of λ_{ex} = 450 nm for CdS and 350 nm for ZnS.

The emission band maximum for CdS is observed between 456 nm and 470 nm at sizes ranging from 2.62 nm to 2.73 nm, fig. 9a and while for ZnS it is observed between 454-466 nm for sizes ranging from 2.88 to 4.09 nm, fig. 9b. Both samples show red shift gradually as the particle size increase.

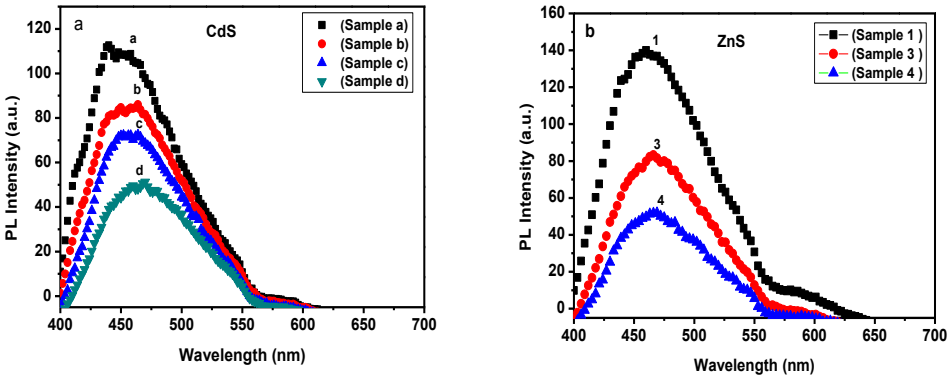

Fig. 9. Photoluminescence intensity of (a) CdS and (b) ZnS nanoparticles at various sizes

Fig. 10 the photoluminescence(PL) spectra of the CdS and ZnS NPs have been determine by strong emission peaks at around 464 nm and 463 respectively . This strong emission is according to deep trap sites which in turn could be traced back to sulfur vacancies. The PL of ZnS NPs is blue shifted (1 nm) compared with the PL of CdS NPs. Interesting result of the work can be seen from PL emission spectra, where the emission intensity of capped ZnS sample is significantly high compared to capped CdS nanoparticles about 3 fold increment in intensity has been achieved, this might be ZnS is optically transparent to the emission range, therefore no photons losses are associated to ZnS with visible light emission [22, 33].

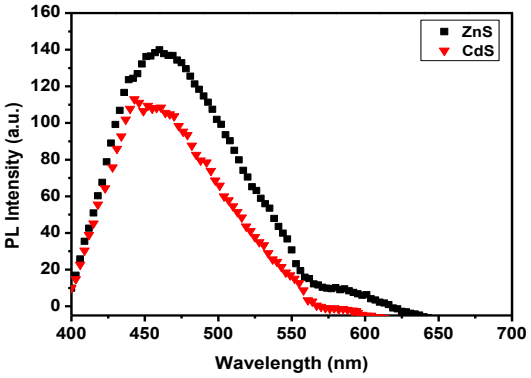

Fig. 10. The PL spectra of CdS and ZnS nanocrystals

4. Conclusions

CdS and ZnS NPs were successfully prepared using an organometallic method. In this study, we concluded that the XRD analysis confirmed that CdS and ZnS NPs were of the hexagonal wurtzite structure. The size of nanocrystalline powder was about 3.34 nm for CdS and about 2.95 nm for ZnS. W-H plot to determine the crystallite size which found was to be 2.02 nm for CdS and 3.73 nm for ZnS. The strain-induced broadening due to lattice deformation was evaluated. TEM images showed the sizes of CdS and ZnS NPs were averaged about 3.5±0.5 nm and 3.75± 0.3 nm, respectively. FTIR and Raman observations for the as-prepared CdS, ZnS NP's were recorded.

Absorption spectra revealed that, the increase in particle size with increasing of growth time ranging from 2.62-2.73 nm for CdS, while ranging from 2.88-4.09 nm for ZnS. We showed that the absorption peaks were red-shifted gradually as the particle size increased with an increment equals 5 nm for CdS and 19 nm for ZnS. The observed E_g of CdS NPs is blue shifted from its bulk value (E_g = 2.45 eV) with increment equals 0.24 eV. As well the E_g of ZnS NPs is blue shifted from its bulk value (E_g = 3.65 eV) with increment equals 0.32 eV. The difference in band gap of the nanoparticles is due to the change in the ground state (bulk) to size dependence. The PL emission was measured for ZnS NPs (excitation at 350 nm) which showed comparatively 3 fold enhancements from CdS NPs (excitation at 450 nm).

Acknowledgements

This work was supported by Aden University (Yemen) and Assiut University.

References

[1] B. Bodo, P. K, Kalita, AIP Conf. proc. **1276**, 31-36 (2010).
[2] D. Denzier, M. Olschewski, K. Sattler, J. Appl. Phys. **84** (5), 2841-2845 (1998).
[3] H. Zhang, X. Chen, Z. Li, J. Kou, T. Yu, Z. Zou, J. Phys. D: Appl. Phys. **40**(21), 6846-6849 (2007).
[4] H. Y. Lu, S. Y. Chu, J. Cyst. Growth. **265**, 476-481 (2004).
[5] H. Peng, B. Liuyang, Y. Lingjie, L. Jinlin, Y. Fangli, C. Yunfa, Nanoscale Res. Lett. **4**, 1047-1053 (2003).
[6] V. Srinivas, S. K. Barik, B. Bodo, D. Karmkar, T. V. Chandrasekhar, J. Magn. Magn. Mater. **320**, 788-795 (2008).
[7] J.P. Borah, K.C. Sarma, Acta. Phys. Polon. A. **114**, 713-719 (2008).

[8] A. S. Lahewil, Y. Al-Douri, U. Hashim, N. M. Ahmed, Solar Energy. **86**, 3234-3240 (2012).
[9] P. A. Chate, P.A.S. S. Patil, J.S. Patil, D. J. Sathe, P. P. Hankare, Physica B: Condens. Matter. **411**(15), 118-121 (2013).
[10] Z. R. Khan, M. Zulfequar, M. S Khan, Mater. Sci. Eng. B. **174**, 145-149 (2010).
[11] A.S. Khomane, J. Alloys. Compd. **496** (1), 508-511 (2010).
[12] R. Seoudi, A. A. Shabaka, M. Kamal, E. M. Abdelrazek, W. Eisa, Physics E. 45, 47-55 (2012).
[13] M. Elango, D. Nataraj, K. Prem Nazee,r M. Thamilselvan, Mater. Res. Bull. **47** (6), 1533-1538 (2012).
[14] P. Alivisatos, Science **271**, 933-937 (1996).
[15] V. N. Soloviev, A. Eichhofer, D. Fenske, J. Am. Chem. Soc. **123** (10), 2354-2364 (2001).
[16] J. I. Kim, D. Jung, J. Kim, C. Nahm, S. Lee, B. Park, Solid State Commun. **152**, 1767-1770 (2012).
[17] C. Y. Wang, X. Mo, Y. Zhou, Y. R. Zhu, H. T. Liu, Z. Y. Chen, J. Mater. Chem. **10**, (2000), 607-608 (2000).
[18] N. L.Pickeet, D. F. Foster, D. J. Cole Hamilton, J. Mater. Chem. **6**(3), 507-509 (1996).
[19] V. Singh, P. Chauhan, J. Phys. Chem. Solids. **70**(7), 1074-1079 (2009).
[20] C. B. Murray, D. J. Norris, M. G. Bawendi, J. Am. Chem. Soc. **115** (19), 8706-8715 (1993).
[21] S. Bai, J. Hu, D. Li, R. Luo, A. Chena , C. C. Liub, J. Mater. Chem. **21**, 12288-12294 (2011).
[22] H. Kumar , M. Kumar ,P. B. Barman , R. R. Singh, Appl. Phys. A **117**, 1249–1258 (2014).
[23] R. Singaravelan • S. Bangaru Sudarsan Alwar, Chem., **4**, 109–117 (2014).
[24] Y. T. Prabhu,K. V. Rao, V. S. Kumar, B. S. Kumari, World J NanoSci. Eng. **4**, 21-28 (2014).
[25] V. D. Mote, B. N. Dole, Advanced Materials Research, **678**, 113-117 (2013).
[26] P. Jakhmola1, P. K. Jha, S. P. Bhatnagar, Appl Nanosci, **6**, 673–679 (2016).
[27] D. Sukanya, P. Sagayaraj, Int.J. ChemTech Res., **7**(3), 1421-1425 (2015).
[28] W. W. Yu, L. Qu, W. Guo, X. Peng, Chem. Mater. **15**, 2854-2860 (2003).
[29] N. K. Abbas, K. T. Al- Rasoul, Z. J. Shanan, Sci. **8**, 3049-3056 (2013).
[30] B. Gündüz, , Polymer ulletin, **72**(12), 3241–3267 (2015).
[31] P. Iranmanesh, S. Saeednia, M. Nourzpoor, Chin. Phys. B. **24** (4), 046104(1-4) (2015).
[32] R. Kalyani , K. Gurunathan, , Kenk Nanotec Nanosci **1**, 1-5 (2015).
[33] H. Kumar, P. B. Barman, R. R. Singh, Int. J. Sci. Eng. Res. **5** (5), 40-53 (2014).